An outline of the synthesis and properties of silicon nanowires

2010 Semicond. Sci. Technol. 25 024003

(http://iopscience.iop.org/0268-1242/25/2/024003)

Semicond. Sci. Technol. **25** (2010) 024003 (16pp) doi:10.1088/0268-1242/25/2/024003

TOPICAL REVIEW

An outline of the synthesis and properties of silicon nanowires

P R Bandaru and P Pichanusakorn[1]

Materials Science Program, Department of Mechanical and Aerospace Engineering, University of California, San Diego, La Jolla, CA 92093-0411, USA

E-mail: pbandaru@ucsd.edu

Received 6 July 2009, in final form 4 August 2009
Published 22 January 2010
Online at stacks.iop.org/SST/25/024003

Abstract
We consider some of the significant aspects of Silicon nanowires (NWs), referring to their various modes of fabrication and their measured properties. Lithographic patterning as well as individual NW synthesis, e.g., through chemical vapor deposition based processes, has been utilized for their fabrication. It is seen that the properties of these nanostructures, to a large extent, are determined by the enhanced surface area to volume ratio and defects play a relatively major role. A diminished size also brings forth the possibility of quantum confinement effects dictating their electronic and optical properties, e.g., where NWs can possess a direct energy gap in contrast to the indirect bandgap of bulk Si. While new challenges, such as enhanced Ohmic contact resistance, carrier depletion – which can severely influence electrical conduction, and surface passivation abound, there also seem to be exciting opportunities. These include, e.g., high sensitivity sensors, nanoelectromechanical systems, and reduced thermal conductivity materials for thermoelectrics. Much preliminary work has been done in these areas as well as investigating the possible use of Si NWs for transistor applications, photovoltaics, and electrochemical batteries etc., all of which are briefly reviewed.

(Some figures in this article are in colour only in the electronic version)

1. Introduction

Silicon has been the mainstay of the semiconductor industry and a harbinger of the microelectronics revolution. The thrust toward continuing miniaturization, via the ubiquitous Moore's law [1], has now extended to exploring the application of the element's nanostructures in various dimensionalities, such as thin films, nanowires and quantum dots. In this paper, we briefly review the distinguishing electronic and lattice properties in one such manifestation of nanostructured silicon [2], i.e. Si nanowires (NWs). A major focus of this article is on whether the NW form confers any special advantages, in addition to reduced size, to enable new fundamental physical insights and practical application. In this context, we will first consider the structure and assembly, through a study of fabricated ('top down') and synthesized ('bottom up') Si NW structures. The enhanced surface area to volume ratio in NWs implies that the surfaces and interfaces play a more important role than in the bulk, and will be considered. The reduced size is also important in altering the fundamental electronic band structure of Si, through quantum confinement effects, which will be explored next. Optoelectronic properties are closely associated with such issues. The implications of nanostructuring on the prevalent use of Si as a photovoltaic material will also be discussed. Subsequently, the properties of the lattice through an overview of the phononic properties will be surveyed. The latter aspect is especially interesting in view of the recent proposal to use Si NWs as thermoelectric materials.

It would be interesting, at the very outset, to consider and contrast Si NW structures with other well-known one-dimensional structures such as carbon nanotubes (CNTs) [3].

[1] Author to whom any correspondence should be addressed.

For example, why are Si NWs more studied compared to Si nanotubes?

1.1. Nanowires versus nanotubes

Generally, a *greater* variety of structures and morphologies is possible in carbon, compared to Si, due to smaller atomic size and higher π bonding energy (∼2.5 eV) in C which enables multiple configurations, e.g. sp^2 orbital hybridization for CNTs and sp^3 hybridization for carbon nanowires. Si, on the other hand [4], has a lower π bonding energy (∼1 eV) which makes sp^2 hybridization and Si NT formation less likely. Consequently, Si maintains the sp^3 configuration, as in the NW form.

However, Si NTs could be caused to form under conditions which promote sp^2 bonding and layer formation, akin to the methods used for synthesizing CNTs [5], e.g. using a DC-arc plasma method to synthesize Si NTs, ∼7 nm in diameter [6]. Alternative methods, e.g. supercritical hydrothermal synthesis [7], have also been used for synthesizing NTs ∼15 nm outer diameter and ∼5 nm inner pore diameter. The latter were proposed to be formed through the introduction of Si–H bonding [7] at the ends which maintains a metastable structure through avoidance of sp^3 bonding. Hydrothermal synthesis also facilitates SiO species which disproportionate to SiO_2 and Si forming Si NTs along the longitudinal direction.

Similar to CNTs, a definite chirality [8] could be identified and the Si NTs could be characterized, experimentally, as metallic or semiconducting. Through first principles calculations, two types of Si NTs were distinguished [9], i.e. (1) *h*-type formed by rolling graphite-like sheets ('silicene' [10]) with sp^2-configured Si, and (2) *g*-type formed through the rolling of (111) surfaces with sp^3-configured Si. It was then calculated that while the *h*-type NTs have properties analogous to CNTs, the *g*-type NTs are more stable and follow selection rules for metallic and semiconducting character *contrary* to those of CNTs. For example, most 'armchair', i.e. (n, n) and zig-zag, i.e. (n, m)-type Si NTs, where n and m are indices of chirality, *with* $n > 5$, *g*-Si NTs are semiconductors and exhibit a decreasing E_g with increased diameter. On the other hand, smaller diameter Si NTs were predicted to be metallic due to the effects of curvature and strong mixing of the π energy levels with the valence band [11].

The study of Si NTs still seems to be in its infancy [4], with large ambiguity in terms of fabrication, properties and possible uses. Much more effort seems to have been devoted to the synthesis and characterization of the NW forms.

2. Synthesis of Si nanowires (NWs)

Si NWs may be fabricated through both 'top-down' approaches, i.e. through lithographic patterning, or 'bottom-up'/chemical synthesis of Si NWs. We will first consider a few methods for NW growth using the former approach and then review the use of chemical vapor deposition (CVD) techniques, exploiting the VLS (vapor–liquid–solid), oxide-growth and solution-phase-based approaches. The section will then conclude with the outline of a method to further reduce Si NW diameters, to enable features of quantum confinement.

2.1. Lithographic patterning of NWs

Traditional lithographic methods, e.g. electron-beam lithography (EBL), can be used to fabricate Si NWs through the use of SOI (silicon on insulator) substrates, with a pre-determined Si thickness on top of SiO_2. The surface is then patterned with electron-beam sensitive chemical resists and the oxide may then be removed through dry or wet etching. Through a careful control of process conditions, e.g. beam currents, reduced system noise, appropriate resist–developer combinations, etc, NWs of diameters as small as 10 nm could be fabricated and practically used for a field-effect transistor (FET) and biosensing applications [12]. The lithographic method can be adapted to the controlled placement of both horizontal and vertically orientated NWs. Direct-write EBL is capable of 10 nm resolution, and the throughput could be increased through wide area projection-based EBL, such as the SCALPEL (scattering with angular limitation in projection electron-beam lithography) system developed by Bell labs [13] or the PREVAIL (projection reduction exposure with variable axis immersion lenses) technology of IBM [14].

Alternatives for the placement of arrays of Si NWs include the nanoimprint lithography (NIL) or the SNAP (superlattice nanowire pattern transfer) method [15]. In the former, masks fabricated through EBL were used to imprint patterns into polymer films [16]. As an interesting variant of this scheme, in the SNAP method, superlattices, e.g. with alternating layers of GaAs and $Al_{0.8}Ga_{0.2}As$, fabricated through molecular beam epitaxy (MBE) were used as templates (figure 1). The SNAP process can be used for NW fabrication from a native wafer of a given stoichiometry, doping and crystallographic orientation. The width of the NWs can be controlled through the thicknesses of the superlattice layers and the NW length dictated by the substrate and can be of the order of millimeters [17]. Si NWs made through this process have been used for thermoelectrics [18], arrays of field-effect transistors (FETs) [19] and electronic devices with more complex architectures, such as crossbar-type electronic memories [20].

Alternately, chemical synthesis of Si NWs, using the 'bottom-up' approach is being extensively used for wafer-scale growth and *in situ* tunability of NW characteristics. We next outline two commonly used approaches using CVD-based processes. At the very outset, the growth of Si filaments/'whiskers', using CVD-based methods, was laid out in the 1960s by invoking the role of impurities on the Si substrates [21]. The impurities were hypothesized to form a liquid alloy with Si, which acts as a sink for species from the vapor phase (e.g. SiH_4). The subsequent crystallization of Si, in the form of whiskers/NWs, from the supersaturated alloy was then proposed to occur through substrate annealing in reactive atmospheres through a vapor–liquid–solid (VLS)-type of mechanism [22].

2.2. The VLS mechanism of Si NW synthesis

This method of Si NW growth is thought to proceed through the following sequential steps [23]: (1) adsorption of Si containing gaseous species on the surface of *molten* metal (e.g. Fe, Au, Ni) nanoparticle catalysts, (2) diffusion of Si through the catalyst,

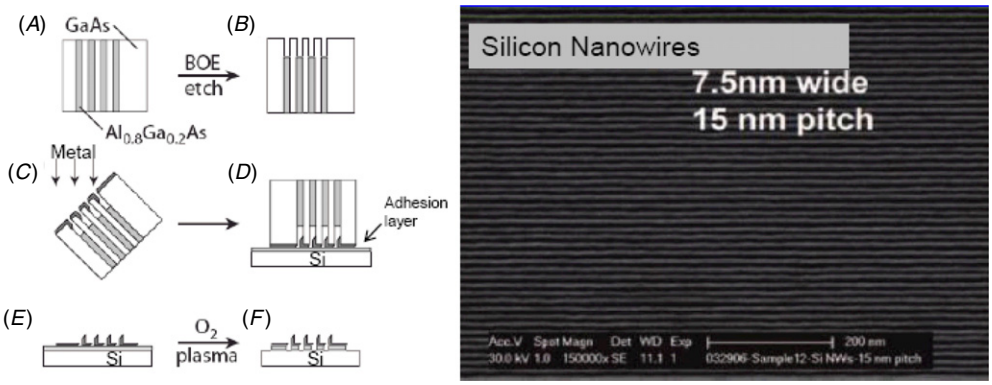

Figure 1. The SNAP method for fabricating Si NW arrays. (*A*) A GaAs/$Al_{0.8}Ga_{0.2}As$ superlattice fabricated by MBE is (*B*) preferentially etched to remove a part of the $Al_{0.8}Ga_{0.2}As$. (*C*) The etched substrate is used as a template for angled deposition of the metal, e.g. Pt or Au, at the tips of the GaAs layers. (*D*) The substrate is then placed in contact with a Si wafer, with the aid of an adhesion layer and then (*E*) released though chemical etching. The metal lines remain on the wafer and serve as masks for etching Si NWs, say through reactive ion etching (RIE). The figure on the right shows a Si NW array made through this process. Figures adapted from [15] and [17].

(3) nucleation and crystallization of Si at the liquid–solid interface and (4) lateral nanowire growth. The diameters of Si NWs synthesized by invoking the VLS mechanism would be dictated by the size of the catalyst particle on the substrate while their length would depend on the duration of growth.

In one prototypical experiment, laser ablation of a $Si_{0.9}Fe_{0.1}$ solid target, at furnace temperatures around 1200 °C, was shown [24] to yield ∼6–20 nm diameter Si nanowires with lengths in the range of 1–30 μm. The high ambient temperature serves to maintain the ablated Si–Fe clusters in a molten state which then condense onto a cooler substrate. The supersaturation of the Si in the Fe was the driving force for the re-precipitation of the silicon, when cooled, in the NW form as illustrated in figure 2. Consequently, the catalyst particle would often be found at one end of the NW.

In the VLS reaction sequence, it was observed that the growth rate was most dominated by the decomposition kinetics of the Si containing gaseous species, e.g. using Si_2H_6 as the gas source results in a 30 μm min^{-1} growth rate while the use of silane (SiH_4) yields a growth rate of ∼1 μm min^{-1}. Such difference could presumably arise due to a larger chemical potential of Si in Si_2H_6 compared to SiH_4 *vis-a-vis* the chemical potential of Si in the NW. As one example of this effect, it was seen that initiation of growth could occur, at smaller NW diameters, by increasing the partial pressure of the Si precursor [25, 26]. The growth rate of Si NWs was found to be a function of diameter, with a larger rate for smaller diameter NWs, and temperature, with a saturation of growth rate being observed earlier at lower temperatures [27]. However, an increased rate of growth would typically lead to the greater incorporation of defects.

Typically, the metals for the catalyst particles are chosen for their ability to form low melting point eutectic alloys with Si, e.g. ∼640 K for Au–Si. The growth temperature could then, in principle, correspond to the eutectic temperature [25]. However, this again typically leads to defective NWs and consequently, higher growth temperatures (>1000 K) along with a slow growth rate (<10 μm h^{-1} [28]) are used to reduce the number of defects. However,

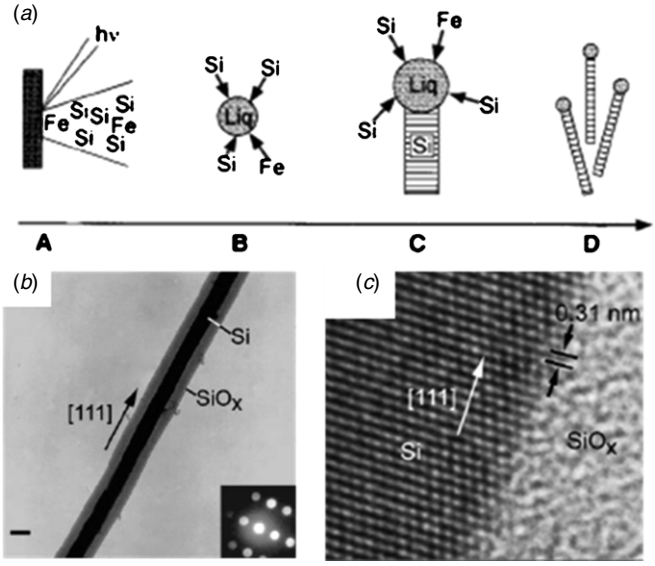

Figure 2. (*a*) (A) Laser ablation of a $Si_{0.9}Fe_{0.1}$ target causes the formation of (B) Si–Fe nanoclusters, which when cooled cause the (C) precipitation of Si in the (D) nanowire forms. Such a VLS (vapor–liquid–solid) growth mechanism, with the characteristic formation of $FeSi_2$ particles at the ends, is thought to be responsible for inducing NWs. The nanowires typically consist of a crystalline Si core surrounded by amorphous SiO_x as indicated by the (*b*) low resolution and (*c*) high resolution transmission electron microscopy (TEM) micrographs. Figure adapted from [24].

at such high temperatures larger catalyst particles form due to Ostwald ripening phenomena [29] and yield NWs >10 nm in diameter. Molecular beam epitaxy (MBE) techniques suffer from such limitations [30] and consequently larger diameter NWs (∼40 nm) [27] are typically synthesized. While relatively defect-free NWs epitaxial to the substrate can be generated, a small growth rate, 150 nm h^{-1} [27], is another shortcoming of MBE-based processes [31]. To bypass such thermodynamic limitations, alternative, non-equilibrium techniques, such as laser ablation, have been attempted to produce smaller catalyst particles and have yielded smaller diameter (up to 3 nm) Si NWs [24, 28]. Additionally, the

eutectic temperature may not correspond to that obtained from traditional phase diagrams, i.e. the liquidus temperature could also be significantly reduced, by as much as 100 K, due to enhanced interfacial energy contributions from smaller diameter catalyst particles [32]. The latter phenomena, e.g. the Gibbs–Thomson effect [29], would also reduce the amount of Si that can be incorporated in the catalyst particle and would further limit the growth of smaller diameter NWs [33]. It should also be noted that the incorporation of Au results in the deterioration of the electrical properties due to its propensity to form deep-level defects [34]. Consequently, several alternative metal catalysts have been attempted for Si NW growth, including Ti [35], Al [36], Cu [37], Mn [38], etc, many of which employ sub-eutectic temperature growth through the VSS (vapor–solid–solid) mechanism, with the catalyst remaining in the solid phase [38].

Typically, gas flow conditions and reaction temperatures can be adjusted for preferential growth of Si NWs in a particular direction, e.g. perpendicular to the substrate. For example, with growth on (1 0 0) Si substrates ⟨1 1 1⟩ oriented Si NWs would be expected to be dominant due to the lower surface energy of {1 1 1}, ∼1.23 J m^{-2} [39]. Experimentally [40], the following diameter distribution versus orientation was noted for Si NWs: i.e. 3–10 nm: ⟨1 1 0⟩, 10–20 nm: ⟨1 1 2⟩, 20–30 nm: ⟨1 1 1⟩. This result would imply that for smaller diameter NWs, alternative higher energy orientations, i.e. with surface energy ∼1.51 J m^{-2} for ⟨1 1 0⟩ [39] or in ⟨1 1 2⟩ [26] are possible. In this context, it was seen that H-terminated Si {1 1 1} surfaces favor the growth of small diameter NWs due to the formation of molten Au–Si alloy droplets in pits vacated by the H [41]. It was then thought that the lower limit to NW diameter was dictated by the size of the Au atom clusters and could even approach ∼1 nm [27]. Consequently, it can be surmised that the minimization of the sum of the interfacial and surface energies could dictate the NW orientation and not the latter alone.

The VLS-mediated synthesis has also been postulated to be a relevant growth mechanism for a variety of other elemental and compound NW systems [42]. In the case of Si NWs, other experiments have implied the role of SiO_x present on the NWs, e.g. due to ambient oxygen, as integral to Si NW growth.

2.3. Oxide-assisted growth mechanism

It was noted that the growth of Si NWs was greatly enhanced when SiO_2 containing Si powder targets were used in laser ablation, compared to (i) a metal-containing target, e.g. $Si_{0.9}Fe_{0.1}$, (ii) a pure Si target and (iii) a SiO_2-based target. It was then proposed that a thermally activated chemical reaction: Si (s) + SiO_2 (s) → 2 SiO (g), generates gaseous SiO species which decompose to Si nanoparticles and agglomerate to form Si NWs [43]. The Si nanoparticles embedded in an oxide matrix serve as nuclei for NW growth. Such a mechanism could explain the formation of linear as well as various nonlinear morphologies of NWs, e.g. spring-like (figure 3(*a*)), periodically interrupted ('fish-bone' type) or wires with a string of catalyst particles ('necklace' type) (figure 3(*b*)), depending on whether single/multiple nucleation sites were involved and whether the growth occurred stably/unstably, respectively [44]. It was also interesting to note that oxide-assisted growth seemed to yield smaller diameter Si NWs (approaching 1 nm) and alternate crystalline orientations, i.e. ⟨1 1 2⟩ and ⟨1 1 0⟩ [44]. Si NWs, formed through such a mechanism, could be converted to the nanotube form, through thermally induced inner Si core melting [45] induced by exposure to intense radiation (∼0.2 J m^{-2}), i.e. a photographic flash.

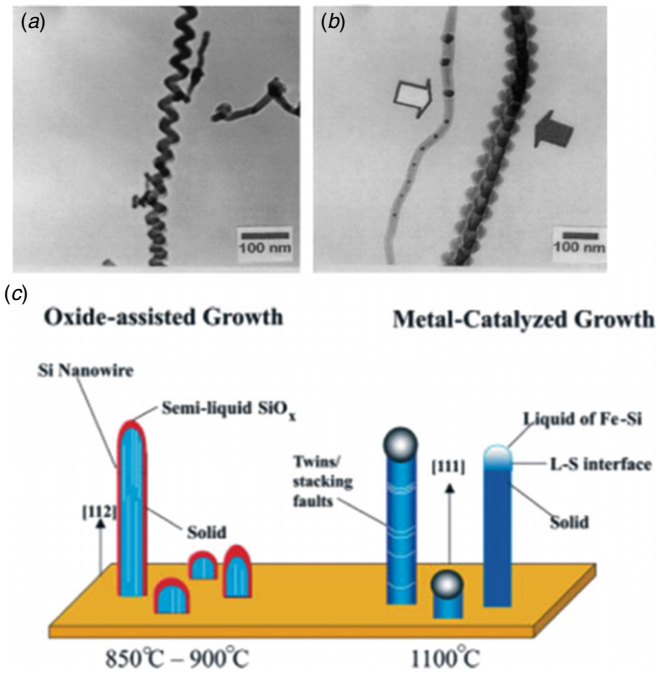

Figure 3. Alternative morphologies such as (*a*) spring-shaped and (*b*) fishbone structures can be obtained through invoking non-catalyst-based oxide-assisted growth. (*c*) In comparison with the VLS method (metal-catalyzed growth), in the oxide assisted growth method, lower temperatures of synthesis can be used leading to smaller diameter NWs with alternative orientations and greater morphological varieties. Figures adapted from [43] and [44].

2.4. Solution-based synthesis for Si NW fabrication

Solution-based synthesis was suggested for large volume, small (mean ∼4–5 nm) and narrow diameter (∼10% standard deviation) growth of Si NWs [46, 47]. One method incorporates reactant supply in the liquid phase giving rise to a SLS (solution–liquid–solid) mode of NW growth [47]. As an example, alkanethiol capped Au nanocrystals were dispersed in supercritical hexane along with a source precursor (mono-phenylsilane [48]/di-phenylsilane [49]) for Si. At temperatures of 500 °C and pressure ∼10^4–10^5 Torr, the precursor decomposes into Si atoms, which dissolve into the Au and are subsequently expelled through supersaturation as NWs. It is seen that generally the overall mechanism is akin to a VLS mode of growth, in that the Au nanocrystal size could dictate the Si NW diameter. However, supercritical fluid pressure could also be used to tune growth orientation by enhancing diphenylsilane degradation. For example, it was seen that increasing pressure, say from 10^4 to 10^5 Torr,

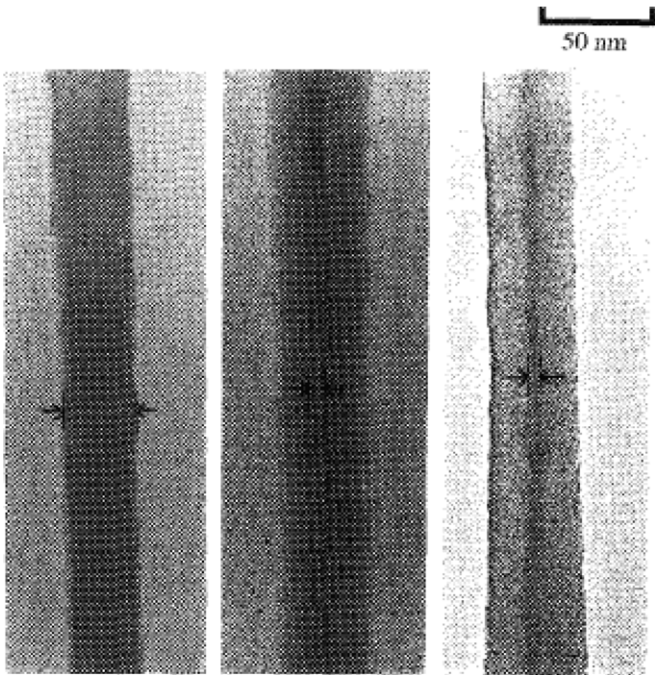

(*a*) (*b*) (*c*)

Figure 4. TEM micrographs of Si columns, fabricated through e-beam lithography and reactive ion etching (RIE), subject to increasing times of dry oxidation, i.e. (*a*) 0 h, (*b*) 8 h and (*c*) 16 h at 850 °C. The initial (*a*) 30 nm diameter is gradually reduced to (*b*) 7 nm and (*c*) 6 nm. Figure adapted from [51].

caused the NWs to change orientation from predominantly ⟨1 0 0⟩ to ⟨1 1 0⟩. Alternative to Au catalysts (see section 2.2), Si NW growth using nanoparticles of Cu [48] and Ni [46] at sub-eutectic temperatures of growth has also been attempted. Issues regarding better control and uniformity of passivation of NW surfaces [47], which result in diminished luminescence efficiency (section 5.1) in chemical synthesis-based growth, are being investigated.

2.5. Reducing the diameter of Si NWs through self-limiting oxidation processes

Si NWs, fabricated through lithographic patterning or chemical synthesis, can be further reduced in diameter through a self-limiting oxidation process [50]. For example, Si rods of diameters ∼20–50 nm fabricated through EBL [50], or NIL [16]-based methods, were subject to dry oxidation at ∼800–950 °C for various times (ranging from 0–15 h). It was then seen that the oxide growth on the Si pillars undergoes a temperature-dependent saturation [51], e.g. at ∼24 nm at 850 °C and 16 h (figure 4). Consequently, with an initial Si pillar diameter of ∼30 nm, a 6 nm Si core can be obtained.

Such a self-limiting oxide thickness is due to the stresses generated due to oxide growth at nonplanar Si/Si oxide interfaces [52] as are found in nanostructures [53]. Consequently, the initial oxide could be under tensile (/compressive) stress due to the convex (/concave) shape of the surface and promote thick (/thin) oxide layers [54]. In the case of oxide films on Si NWs, the elastic energy increases with increasing thickness and at a certain value—the self-limiting thickness—it is larger than the energy required for ambient oxygen to diffuse and oxidize the inner Si.

An alternative method to reduce the Si NW diameter exploits electrochemical reactions [55], as are used for the synthesis of porous Si. In this case, fluoride ions in HF oxidize the Si and dissolve the surface layers. The extent of oxidation can be controlled through monitoring the current through the NW and can be tuned through the Si doping, concentration of electrolyte, etc.

As with most other nanostructures, the controlled growth and placement of chemically synthesized Si NWs is quite challenging. While the CVD-based methods provide vertically oriented NWs on a substrate, there are obvious issues associated with electrically contacting the top surfaces. Consequently, various strategies have been used and are in development for directed and controlled growth [56] and/or assembly of Si NWs. This includes, for example, (a) *in situ* growth [57], (b) fluid-assisted assembly [58], (c) alignment based on their polarizability [59] using localized electric fields (>1 V μm^{-1}) [60], etc.

3. The influence of interfaces and defects

The enhanced influence of the surface area to volume ratio in Si NWs leads to an exaggerated importance for interfaces, defects and issues such as surface reconstruction and passivation. As an example, from a consideration of the total energy of the NWs, including the surfaces and the facets in addition to the bulk energy, it was predicted that a *polycrystalline wire* with fivefold symmetry would have the lowest energy for NWs of diameter <6 nm [61]. While such predictions imply that small diameter Si NWs could be intrinsically metastable, such morphology does not seem to have been experimentally observed to date.

3.1. Interfacial defects and passivation

At the very outset, there is a change in atomic coordination of the Si from the bulk (four-fold coordination) to the surface (with lower coordination), which leads to the possibility of reconstruction of bonds at the surface. However, it is typical of Si surfaces processed in the ambient to develop an oxide coating on the surface with associated fixed and mobile charges [62]. An increased trap density, compared to that in oxide formed on planar surfaces, has been inferred through conductive atomic force microscopy (AFM) [63] on Si NWs. Typical to a Si/SiO$_x$ interface, one must consider (1) *mobile charges*, e.g. Na$^+$ ions, introduced as contaminants during processing, (2) *trapped charge in the oxide* constituted from Si and oxygen dangling bonds, i.e. Si• and SiO$^-$, respectively, which could be brought about by exposure to high-energy electrons, (3) *fixed oxide charge* due to unsatisfied Si–Si and Si–O bonds, the density of which is dependent on ambient oxidation conditions and wafer orientation, e.g. $\sim 10^{10}$ cm^{-2} on (1 0 0) Si surfaces and $\sim 5 \times 10^{10}$ cm^{-2} on (1 1 1) Si and (4) *interfacial charge density* localized within 0.2 nm of the Si/SiO$_x$ interface.

The presence of interfacial charges and defects, in addition to other defects intrinsic to the bulk of the NW surface, can substantially influence electrical and thermal transport [64] through both electron and phonon scattering [65]. These influences can be manifested, e.g., through (i) a reduced electrical carrier mobility, (ii) hysteresis and non-reproducibility in the current–voltage (*I–V*) characteristic curves, (iii) enhanced optical luminescence, (iv) enhanced piezoresistance coefficients [66], (v) lowered thermal conductivity in thermoelectrics [65], etc.

Surface states and interfacial charges could be *amphoteric*, i.e. behaving as acceptors, when their energy levels are situated in the upper half of the bandgap, or as donors when their energies are in the bottom half of the bandgap. In these cases, there is also the possibility of electrical carrier depletion—sometimes extending through the NW diameter. Consequently, charged states and defects which are acceptor-like or donor-like have to be passivated to shift their energy levels into the conduction and valence bands, respectively. It was seen, for example, that the hole mobility of boron doped p-Si NWs was enhanced through surface treatment with tetraethyl ammonium bromide solutions [67], which affected passivation. Principles analogous to those applied for CNTs [68], where electrons transfer from/to the surface states [69] from attached organic substituents, could also be used.

Generally, adopting careful processing and annealing procedures can reduce the effects of mobile and trapped oxide charge. It is then also indeed fortuitous that Si surfaces are amenable to yield low surface defect densities, of the order of 10^7 cm^{-2}—the lowest of *any* semiconductor [70]. This is accomplished through Si surface passivation using HF acid etching to yield Si–H-terminated surfaces. The effect of hydrogen passivation is best manifested through a change in the density of states (DOS) of the Si NWs (figure 5) [71]. The H was seen to bind to the surface defects (situated in the bandgap) through covalent bonding. Concomitantly, there was a considerable increase in the electrical resistance and ultimately a cut-off of the electrical conduction. Such extreme sensitivity to hydrogen has been proposed for sensor applications.

However, the presence of hydrogen can also lead to the undesirable passivation of donors and acceptors [72] resulting in carrier depletion at the surface. It has been noted that such passivation could extend to NWs with a μm scale diameter. While annealing at ~400 °C would be helpful in restoring the bulk Fermi energy (E_F), higher temperature annealing could result in the formation of H vacancies and surface reconstruction with a pinning of the E_F [64]. A consequent strong energy-dependent scattering could then induce a transition of electrical conduction from the Ohmic to carrier localization-dominated regime.

3.2. Influence on Si NW characteristics

Both from a thermodynamic and practical perspective, the presence of defects in Si NWs is inevitable and exerts a major influence on both electronic and lattice properties. For example, if Si NWs were to be used for transistors/switching devices [67], both extrinsic and intrinsic defects could influence the characteristics through effects such as a change in the threshold voltage [68], reduced carrier lifetime [73], etc.

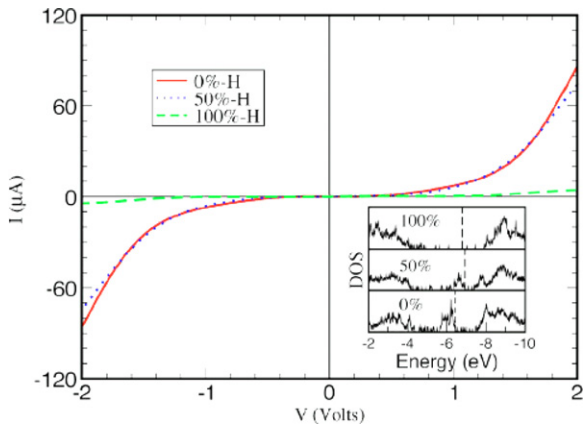

Figure 5. Calculated current (*I*)–voltage (*V*) curves for Si nanowires, with decreasing electrical conduction with enhanced hydrogen content. The inset (dotted line: Fermi energy, E_F) shows that the introduction of hydrogen removes many of the gap states. Figure reproduced from [71].

However, defects do not seem to contribute to a deterioration of the mechanical properties in NWs, e.g. elastic/bending modulus, compared to the bulk values. In fact, *in situ* AFM characterization has revealed [74] that theoretical cohesive strengths, close to 10% of the elastic modulus [75], could be approached in short length (<600 nm) NWs. The influence of surface states has also been implicated in the 40-fold enhancement of the piezoresistance coefficient of Si NWs [66], compared to bulk values. The piezoresistance was shown to be increased through hydrogen passivation (using a HF treatment) and diminished with oxide formation (through HNO_3-mediated oxidation). While comprehensive explanations of these observations are still awaited, the increased influence of strain and defects at such size scales is speculated.

Enhanced biochemical/molecular sensing seems to be feasible through the attachment of singular [76] atomic/molecular moieties to defects on Si NWs, as also observed for carbon nanotubes [77]. The underlying principle is the large surface area with an accompanying greater degree of change of electrical conductance—which is increased with decreasing NW diameter [76]. Additionally, electrochemical processes occur with a greater rate constant [78] enabling mass-transfer-limited reactions with greater sensitivity compared to planar surfaces [78]. Defects also enable selective functionalization through a control of the type and amount of charge on the surface, e.g. through silanization of oxidized Si NWs [79], using compounds such as APTES (aminopropyltriethoxysilane) or OTS (octadecyltrichlorosilane). Negative (/positive) surface charge can enhance (/reduce) the transit current in a p-type Si NW and can be used to tune electrical conductance and even cause a shift of the threshold voltage for current onset [68]. Additionally, the attachment of chemical moieties, e.g. ssDNA, to the functionalization agents and the consequent

electrical current modulation also serve for sensing purposes [79]. Si NWs have also been shown to serve as templates for silica nanotubes [80] with relatively charge insensitive surfaces. Such nanoporous structures could be used for separation at the molecular level, through both size selectivity and electrochemical activity related to the aspect ratio, as evidenced through experiments on DNA translocation [81].

4. Electronic properties

A fundamental modification of electronic properties from the bulk can be evidenced in Si NWs. For example, the indirect bandgap (E_g ~1.1 eV) between the conduction band (CB) minimum and the valence band (VB) maximum, characteristic of bulk Si, could be modified to a direct bandgap due to quantum confinement effects. In addition to such intrinsic effects, surfaces and defects also play a role, e.g., through exerting a greater influence on the valence band states (formed from p-orbitals) of the NWs, which are more localized compared to the conduction band states (formed from *s*-orbitals) [82].

4.1. Modification of the energy bandgap (E_g) and effects of quantum confinement

Motivated by the emission of light from Frenkel defect centers, i.e. C substitutional–Si interstitial pairs in bulk Si [83], the possibility of modification to the electronic E_g in lower dimensional Si structures was investigated [84]. It was then seen that, in Si monolayers terminated with H atoms, the electrical carrier confinement implies that a relatively constant energy would be needed for electron excitation, i.e. the *indirect* energy bandgap would be similar to the *direct* E_g. A direct bandgap is also made more feasible by the presence of electronegative atoms, e.g. O, F, Cl, etc which favor electron excitation in the absence of phonons, i.e. lower the direct bandgap energy relative to the indirect bandgap energy. The enhanced coupling/interaction between the valence and the conduction band in lower dimensions, e.g. Si NWs, has been interpreted in terms of zone-folding. This means that the CB minimum, normally situated along the ⟨1 0 0⟩ direction of the Brillouin zone (near the X-point) is folded back to be in proximity to the VB maximum at the center of the Brillouin zone (near the Γ point)—figure 6 [85].

Molecular dynamics calculations have predicted that an indirect to direct energy bandgap transition occurs in the 4.5–5.3 nm range for Si NWs oriented in the ⟨1 1 1⟩ direction [71], while smaller diameters (in the 1.4–2.1 nm range) have been posited for ⟨1 0 0⟩ oriented NWs [86]. Now, the CB minima of bulk Si at the X-point, i.e. along ⟨1 0 0⟩, has six equivalent valleys which are represented through anisotropic ellipsoids due to the different longitudinal ($m_l = 0.19\ m_e$) and transverse ($m_t = 0.92\ m_e$) masses. Consequently, the projections of the [1 0 0] oriented longitudinal and transverse valleys along the [1 0 0] NW axis are finite and the bandgap remains indirect, while the [0 1 0] and [0 0 1] valleys project on the zone center, yielding a *direct* energy gap between the bands constituted from these valleys and the VB maxima.

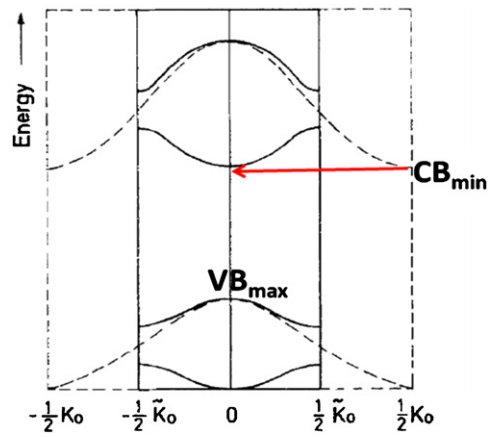

Figure 6. The bandstructure of bulk Si (*dotted line*) is modified (*solid line*) due to enhanced coupling between the valence and conduction bands in lower dimensions. The consequent zone folding as represented by the movement of the conduction band minima (CB_{min}) to the zone center causes greater interaction with the valence band maxima (VB_{max}) yielding a bandgap that is quasi-direct. Figure adapted from [85].

The dependence of the energy gap on size and dimensionality has also been calculated [87] by density functional theory (DFT) in the local density approximation (LDA), with a self-energy correction of 0.6 eV, and shows a monotonic increase with decreasing length scale/confinement parameter ($1/d$), as depicted in figure 7(*a*). The experimental proof of such a bandgap increase was obtained through scanning tunneling spectroscopy (STS) measurements [88] on Si NWs with diameters in the 1.3–7 nm range, as illustrated in figure 7(*b*) [89]. The agreement between theory and experiment is remarkable.

4.2. Doping in Si NWs

There seems to be a general consensus through experimental observation that Si NWs are semiconducting at all sizes and can be doped [90] n-type or p-type, in a similar manner to bulk silicon. Controlled doping, spanning a range of carrier concentrations, can be carried out through reactive gas flow (e.g. B_2H_6 for p-doping and P for n-doping Si [90]) in CVD processes or through ion implantation [91, 92]. Carrier depletion, due to the capture of electrons and holes by surface states and/or defects, is a major issue and results in a reduction from the expected value of the electrical carrier concentration. In very small diameter NWs (~3 nm), there is an additional tendency for dopants to segregate to the surface where they could combine with defects due to the lower formation energies associated with the surfaces [93]. However, the difference in formation energies among surface and core substitutional sites is diminished for larger diameter NWs.

In the context of carrier depletion, it is commonly understood [94] that the Shockley–Reed–Hall (SRH)-type recombination [73] mechanism which involves electrons/holes interacting with a localized state is dominant at low to moderate carrier concentrations. At higher carrier concentrations ($>10^{17}$ cm^{-3}–10^{18} cm^{-3}) [95], Auger

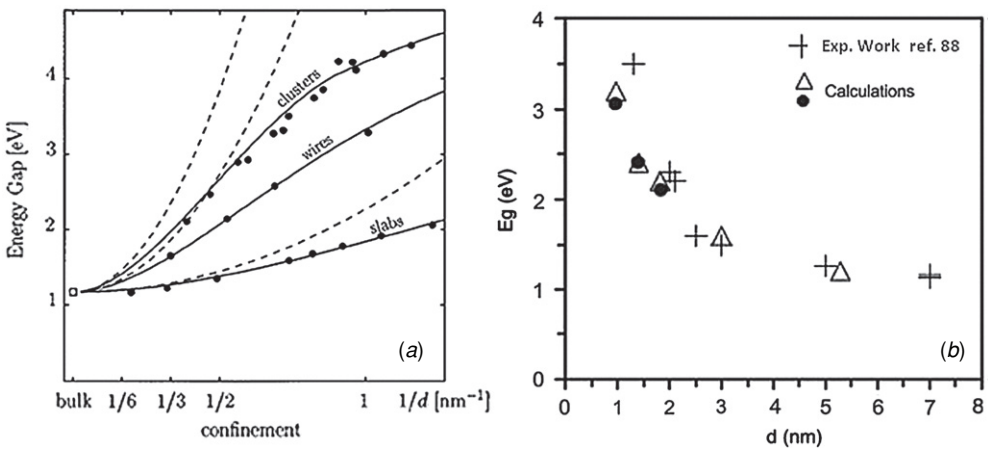

Figure 7. (*a*) The influence of quantum confinement in increasing the electronic energy gap (E_g) from the bulk value (∼1.1 eV) obtained through DFT calculations. Figure adapted from [87]. (*b*) Experimental measurements of the E_g variation with Si NW diameter as inferred through scanning tunneling spectroscopy (STS). Figure adapted from [88]. Calculations refer to the computational predictions from [87] (triangles) and [89] (dark circles).

recombination would also play a role. The Auger mechanism involves the interaction of three carriers, e.g. the energy released by an electron and hole recombining is given to an electron or hole. However, an order of magnitude enhancement in the Auger recombination has been measured in hydrogen-terminated Si (111) surfaces, even at carrier doping $\sim 3 \times 10^{15}$ cm^{-3} [96]. Such an increase suggests that when the extrinsic defect density, which is exaggerated in Si NWs due to the surface states, contributing to SRH-type recombination is minimized, alternative recombination mechanisms could become more important.

In addition to the use of the Hall effect to probe the type of doping and concentration of carriers, alternative techniques such as local electrode atom probe (LEAP) tomography [97] and Raman spectroscopy [98] have been used to probe the effects of doping and crystalline character in Si NWs. In the LEAP method, applied electric fields cause the evaporation of ions from a vertically oriented NW and the ion mass/charge ratio is determined through time of flight measurements. The sequential measurement of ions through the length of the NW yields the distribution of species along the NW to ppm accuracy. Raman scattering probes the inelastic scattering of photons by elementary excitations (e.g. electronic, electron–phonon, etc) in a material and yields information on the excitation energies along with the structure and bonding in the solid [99]. For example, the intensity of the Raman peak can be fitted to yield a typical diameter for the crystalline core of the Si NW. The presence of electrons (/holes) would yield a down (/up) shift of the undoped Si optical phonon peak, from the bulk value of ∼520.1 cm^{-1}, along with low (/high) frequency asymmetry of the peak. Such variation could be understood through the effects on bonding whereby excess (/deficit) electrons would increase (/decrease) the average bond length and diminish (/enhance) the vibration frequency. The additional influence of surface states, which can also serve as acceptors/donors, could also exacerbate the peak shifts [77, 100].

Any residual strain, e.g. due to amorphization induced by ion implantation, can be seen through the symmetrical displacement of the peak. In this case, Raman spectroscopy was used to show that high temperature annealing (>800 °C) was successful in restoring the crystalline character of the ion-implanted Si NWs [92], through observing the peak displacements. The substitution of B atoms into the Si sites (for p-*type* doping) and their electrical activity were also seen through Fano broadening of the Raman peaks [98] which arise due to the coupling of the optical phonons with the hole excitations from the B doping. The observation of local vibrational modes, e.g. due to substitutional atoms and added moieties such as H atoms, in Raman spectra provides an additional level of diagnostics.

4.3. Electrical conduction mechanisms

If carrier depletion is present at the surface, electrical conduction takes place through the bulk of the NW by diffusion of electrical carriers and can be described through the Boltzmann formalism [101]. An experimental understanding of the electrical conduction mechanisms is often obtained through the placement of NWs as carrier channels in the MOSFET (metal oxide semiconductor field effect transistor [34]) configuration. In this case, the carriers (electrons/holes) move from a source to a drain through the NW channel whose conductivity is modulated by a metal gate separated from the channel by an insulating oxide. For channel lengths >10 nm, the effects of carrier tunneling between the source and drain can be ignored [102]. In studies on Si NW-based MOSFETs [67] with channel lengths of the order of 50 nm and NW diameters around 10 nm [103], it was seen that classical electrostatics was adequate to explain the transistor characteristics.

A systematic variation of the active conduction length in undoped Si NWs was accomplished through the controlled fabrication of nickel silicide contacts, which could be diffused to different lengths along the NW through enhanced temperature annealing [104]. It was observed that for NW lengths <1 μm, the electrical transport was limited by the Schottky barriers at the metal–semiconductor interface,

while for lengths >1 μm, an *exponential* drop in the on-current (I_{on}) was seen. The latter could plausibly be due to the presence of defects and strain along the length of the NW (as discussed in section 3). Consequently, in the shorter NWs, the on-state current (I_{on}) was constant and a current modulation, i.e. I_{on}/I_{off}, of $\sim 10^7$ was seen. Such a dependence could be traced to the one-dimensional nature of the carrier transport where defects/impurities can induce a strong resonant backscattering and reduce carrier mobility [105]. Coaxial structures where either the core or shell is doped can be effective in reducing carrier-scattering effects. While discussing electrical conduction through Si NWs, it should be mentioned that their interfacing to external circuitry through Ohmic contacts is non-trivial [106]. In this context, the specific contact resistance (r_C) at a metal–Si interface was theoretically shown to have a lower limit of $\sim 10^{-9}$ Ω cm^2 [107]. Experimental observations have shown that for even optimally doped NWs, the r_C values are two to three orders of magnitude higher [108]. This would imply for a 10 nm diameter Si NW, a contact resistance ($R_c = r_C/A$, where A is the contact area $= \frac{\pi}{4}(5\ nm)^2$) of the order of 5 kΩ and which increases with decreasing Si NW diameter. Additionally, as such low r_C values are obtained at high doping concentrations ($>10^{20}$ cm^{-3}), there is a greater scope for electrical carrier interactions which adversely affect the carrier mobility.

Alternatively, when quantum confinement effects are prevalent, ballistic/non-diffusive transport can occur in the NWs. In the ballistic case, for example, the carrier mean-free path is larger than the channel length. The motion of electrical carriers in the individual sub-bands or energy levels must be considered and the determination of the electrical conductance would involve the solution of the Schrödinger equation [102]. The quantization of electrical carrier energy leads to a discrete variation of the electrical conductance in units of $\frac{2e^2}{h}$ ($\sim$77 μS). Such effects have been seen in p-doped Ge core (10 nm diameter)/Si shell (2–5 nm) NWs, through a quantization of the energy levels in the Ge quantum well.

Finally, conduction through the surface states (section 3.1) with energy levels in the bandgap provides an alternate channel for electrical transport. While simulations have shown [71] that the current–voltage (*I–V*) curves are unaffected by surface reconstruction, the possibility of edge state conduction mediated through surface states [109] resulting in locally inhomogeneous current distribution has been posited.

5. Optical properties

The possibilities of quantum confinement and a *direct* energy bandgap (section 4.1) could modify the optical properties of Si NWs from those in the bulk. In this section, we will consider the characteristics relevant to NWs and their widely touted usage as solar cell materials.

5.1. Effects of quantum confinement in small diameter NWs

Generally, bulk Si is considered to be inefficient as a light emitter (or as a photodetector) due to the indirect energy bandgap, which means that electron–hole recombination for light emission is facilitated through lattice vibrations/phonons. The three-particle requirement along with the lower electron–hole pair (exciton) coupling is the main impediment for enhanced efficiency. In the case of a direct energy bandgap, as can be obtained in Si NWs, larger optical coupling (two orders of magnitude greater than that of an indirect bandgap) is possible between the VB maximum and the CB minimum and luminescence can be obtained. Additionally, with NW diameters below the exciton Bohr radius of $\sim$4 nm for Si [110], quantum confinement effects would be expected to be more prominent. While photoluminescence (PL) measurements can be direct evidence of quantum confinement, it has also been posited that a broadening of the Si peak (at 520 cm^{-1}) linewidth in Raman spectroscopy, from a bulk value of $\sim$5 cm^{-1} to $\sim$50 cm^{-1}, could also be indicative of confinement [26].

The enhanced exciton coupling in direct bandgap Si NWs is also indicated through orders of magnitude increase in the exciton oscillator strength—a measure of the overlap of the electron and hole wave functions, which was shown to scale as 1/(NW diameter)^5 [86]. Consequently, a 0.8 nm diameter Si NW was computed to have the same oscillator strength or luminescence efficiency as bulk GaAs. The exciton binding energies are also enhanced to >0.1 eV in NWs and stable emission may be obtained at room temperature. In one experiment, peaks in the PL spectra were observed for 5 nm and 7.3 nm diameter Si NWs at around 1.8–2.0 eV while an additional peak at $\sim$4.2 eV was seen for a 4.5 nm NW. While the former are more characteristic of indirect bandgap NWs [111], the peak at 4.2 eV is close to the expected value for the direct bandgap at the Brillouin zone center [89] and indicates quantum confinement. The Si NWs, in this case, were synthesized in porous silica through a supercritical fluid-based (incorporating a mixture of diphenylsilane and CO_2) technique. The intimate bonding of the NWs to the surrounding matrix was thought to reduce the effects of surface reconstruction and possible influence on the PL as often invoked in discussing emission from porous Si [112]. The possibility of PL due to transitions between strain-induced (from the surrounding matrix) surface states was also proposed as a way to tailor the wavelength of the light emission. Additionally, it has been seen through electron-energy loss spectroscopy (EELS) for smaller diameter NWs that surface plasmons at the Si–SiO_2 interface could contribute to an enhancement of the direct inter-band transitions [113]. Generally, as excitonic effects are temperature dependent, PL intensity measurements along the length of the NW under a temperature gradient, as was done for GaN NWs [114], could be used to probe the characteristics of the surface and their influence on the luminescence.

5.2. Optical properties of larger diameter Si NWs for photovoltaic applications

In larger diameter (>5 nm) NWs, quantum effects are negligible and the optical properties can be understood through analogy with bulk Si properties. Such materials have been discussed with respect to their use in photovoltaic (PV)

applications [115] which have been discussed in much detail elsewhere [116]. We consider a few salient issues. Generally, the optimal direct E_g for solar energy conversion using PVs is ∼1.4 eV [117]. However, Si with an indirect E_g of ∼1.1 eV in a p–n junction form is often preferred due to its relatively wide abundance, mature technology and low cost [116]. Additionally, bulk Si has relatively low light absorption efficiency, with an absorption coefficient, α, at 550 nm—the peak of the solar spectrum of ∼5830 cm^{-1} [118] in comparison to GaAs with an $\alpha \sim 6 \times 10^4$ cm^{-1}, due to its indirect bandgap. These α values imply that for 90% absorption, approximately 100 μm thick Si would be needed [119]. Consequently, Si NWs which could exhibit absorption greater than a solid Si film [120] due to multiple reflection-induced light trapping are relevant and have been studied for PVs. Another motivation was that NWs could allow for the use of relatively impure Si as it was proposed [115] that the large surface area concomitant with the small carrier diffusion length would improve light exposure and transduction to electrical power, respectively.

Generally, when a medium of refractive index, n (e.g. $n_{Si} \sim 4.077 + 0.028i$ at 550 nm), is in equilibrium with the external black body radiation directly from the sun, there is an enhancement in intensity and absorption, in the medium, by a factor proportional to n^2. Such an increase is due to an increase in the density of states (DOS) which is proportional to k^2, where k $(=\frac{n\omega}{c})$ is the wave vector [121]. In the case of NWs, additional variables such as the geometry (length, diameter, pitch) would also need to be considered in determining the absorption. For example, the number of NW–photon interactions could decrease with increasing energy in contrast to absorption in a thin film. At low photon energies (sub-bandgap), absorption from the surface states also needs to be taken into account. While regularly arranged/ordered Si NWs (>50 nm diameter) have low reflectivity (<20%) over the 350–800 nm spectral range [120, 122] due to strong light trapping and scattering, it was noted [123] that disorder in the NWs could enhance the reflectivity—approaching 90% at $\lambda =$ 800 nm.

Using principles common to bulk/thin film solar cells, attempts were made to fabricate p–n junctions in NWs to enable charge separation and power generation. This was most commonly done through (1) the assembly of n-doped NWs on p-type substrates [124], (2) vertical structures with p- and n-junctions on either ends of the wire [125] or axial p–i–n junctions [126]. However, the small junction area and exaggerated charge depletion effects (section 3.1), both transverse and longitudinal to the NW, make such topologies unattractive [127]. Alternatively, arrays of the radial p–n junction NWs, each with a core (p-type)–shell (n-type) structure [128]—figure 8 [115]—were fabricated. In the core–shell NW structures, it was determined that if (a) the radius of the p-core is approximately equal to the minority carrier diffusion length, (b) the core and shell regions have a sufficiently high doping concentration to avoid depletion and (c) there is a low trap density in the depletion region ($<10^{15}$ cm^{-3}), then PV efficiency could be optimized. Combined with the requirement of

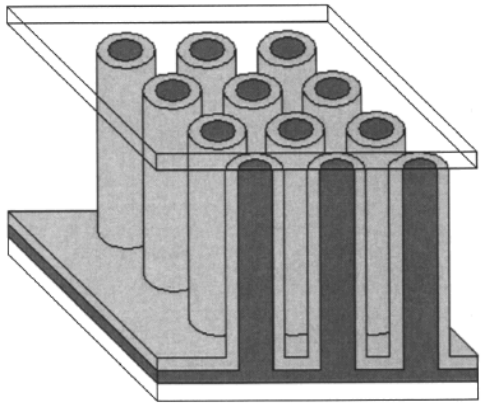

Figure 8. Schematic illustration of a radial p (*dark* gray)–n (*light* gray) junction-based Si NW photovoltaics. Figure adapted from [115].

achieving a low contact resistance, the above conditions stipulate that Si NW diameters could be in the 100 nm to 2 μm [129] range. It was also interesting to note that the specific shape of the Si NW could be important [129] as garnered through measurements on a single 900 nm diameter hexagonal faceted Si NW, where the p–n junction was constituted of a n-type Si NW with the p-side facilitated through Al contacts.

The reported efficiencies of Si NW-based solar cells are at present quite low, ranging from 0.1%[124] to 3.4% [128] for p–i–n structures to 9.31% for n-type Si NWs on p-Si substrates [122]. However, there seems to be scope for improvement through the use of heterojunction and hybrid structures [118] and methods to enhance light absorption [130]. For example, infiltrating voids between the NWs with higher index media, e.g. ethanol with an index of 1.36, was proposed to improve absorption through an increased light scattering mean free path [131]. Additionally, using a gradual change of refractive index from the top to the bottom of the NW array could minimize abrupt reflection [132], i.e. at normal incidence, 98% of the incident light was found to be absorbed through the use of Si nanocone arrays (tapering from 20 nm at the top to 300 nm at the bottom) in comparison with the 85% light absorption for Si NW arrays and 78% absorption for thin films. It would also be interesting to consider whether recent results [133] in the enhancement of the refractive index, due to birefringence in anisotropic media, can be applied to increase light trapping in Si nanowire media.

6. Electrochemical properties

In this section, we consider the unique advantages and possible use of Si NWs as electrodes in lithium (Li) ion batteries. While elemental Li has the highest theoretical specific energy density (∼3860 mAh g^{-1}) [134] due to its low atomic number, its intrinsic instability necessitates the use of Li compounds, such as LiC_6, with a lower energy density (<500 mAh g^{-1}), as anodes in Li-ion-based batteries [134]. In the context of Li-based compounds, it has been known that lithiated Si anodes, in the $Li_{3.75}Si$ form, could have much higher theoretical specific

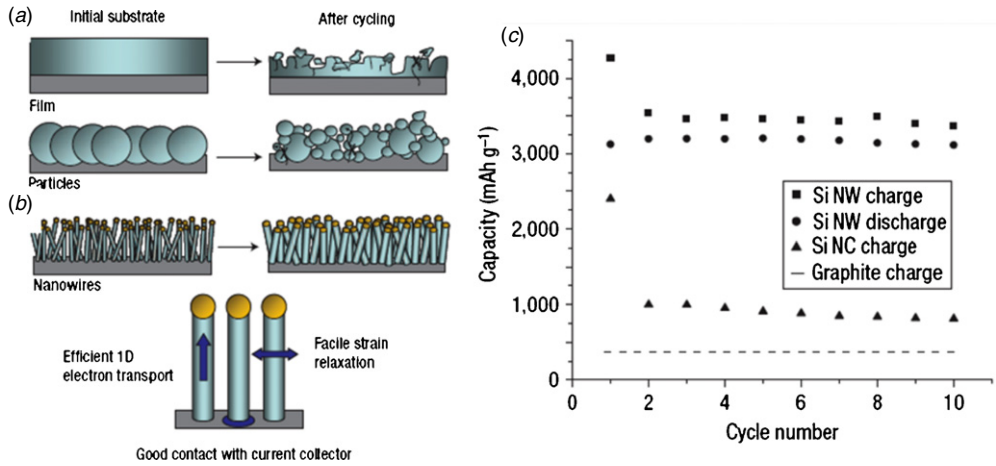

Figure 9. The insertion of Li into Si (*a*) thin films or particles is accompanied by a large volume change and loss of integrity of the anode material. However, (*b*) Si NWs are less susceptible to catastrophic failure. When grown on conducting electrodes, the parallel electrical transport and relative immunity to volume expansion allows for high efficiency. (*c*) Subsequent to a loss of capacity, after the very first cycle, Si NW anodes were seen to be relatively stable and exhibit much higher capacities compared to the presently utilized Li–C (graphite) electrodes. Figure adapted from [139].

energy densities of the order of 3600 mAh g^{-1} [135]. However, poor performance in the charge–discharge characteristics due to (i) a crystalline–amorphous phase transition, along with (ii) the large volume expansion [136] attendant on the insertion of 3.75 moles of Li into 1 mole of Si, results in enormous loss of capacity, even after one cycle. It was then suggested that Si-based nanostructures, such as nanoparticles [137], amorphous thin films [138] or nanowires [139], could be used to overcome the above disadvantages—essentially due to a relatively lower change in the volume for smaller sizes. It was found, in the case of Si NWs, that the Li insertion was less catastrophic compared to particles or films. Additionally, when the NWs were synthesized on conducting substrates, e.g. stainless steel [139], parallel charge transport through a large number of NWs facilitates comparatively greater contribution to energy density.

These advantages of Si NWs were further exemplified through a comparison of the morphology changes in figures 9(*a*) and (*b*) for thin films and NWs, respectively. In experiment, it was found that after an initial decrease after the first cycle of operation (figure 9(*c*)), the capacity was relatively constant at ∼3000 mAh g^{-1} for up to ten cycles. The structural integrity of the NWs was preserved, albeit with a swelling in the NW diameter from ∼90 nm to ∼140 nm (figure 9(*b*)). The formation of amorphous phases due to the Li insertion along with two orders of magnitude decrease in the electrical conductivity was also observed. Crystalline–amorphous core–shell Si NWs, synthesized through modulation of Si NW growth, have also been proposed for anodes. In this case, the crystalline core serves for mechanical support while the external amorphous shell (constituting 98–99% of the total Si NW volume) stores Li ions [140]. An improved cycle number (>100 cycles) along with high rates of charging and discharging was observed for the core–shell NWs.

7. Phononic properties

The characteristics of the Si NW lattice influence both the electrical transport and thermal conductivity (κ). The interactions of the lattice vibrations (phonons) with electrical carriers modulate electrical transport, e.g. through phonon drag, and could reduce carrier mobility. Orders of magnitude reduction in the κ, from the bulk value, was observed in Si NWs and finds potential uses in heat insulation and thermoelectric applications.

7.1. Electron–phonon interactions

The scattering of electrical carriers (electrons/holes) by phonons can simply be probed through considering the resistance (R) variation with temperature (T). For example, a variation of the form $R = A\,T^{3/2} + B$, where A and B are constants, was experimentally observed [141] in p- and n-Si NWs (diameter ∼25 nm, and doping levels $>10^{19}$ cm^{-3}). Such dependence implies bulk electron–phonon scattering and that the electrical transport can be modeled through bulk diffusive transport. The depletion of carriers at the surface (see sections 3.1 and 4.2) seems to preclude the influence of carrier scattering by surface phonon modes.

The sweep of the electrical carriers by the phonons, which is increased when the respective heat flow contributions/energies are comparable [142], is often referred to as phonon drag [143]. Phonon drag effects are most prominent at low temperatures, i.e. <100 K for Si [144, 145]. While this phenomenon inevitably leads to reduced carrier mobility, such effects are frequently invoked in the creation of additional thermoelectric voltage. While the magnitude of such voltage is small in metallic materials ($<5\ \mu$V K^{-1}), orders of magnitude larger contributions can be obtained in semiconductors [146] typically at doping levels $\leqslant 10^{15}$ cm^{-3}, e.g. 5–20 mV K^{-1} at $T < 20$ K in Si [147]. Generally, the contribution to the phonon drag thermopower,

S_{ph-e}, is directly proportional [146] to the ratio of the phonon relaxation time ($\bar{\tau}$) and the carrier relaxation time ($\bar{\tau}_e$) along with the fraction (f) of carrier momentum lost to the phonons, through $S_{ph-e} = \pm m^* v^2 \left(f \frac{\bar{\tau}}{\bar{\tau}_e}\right)$ and decreases with increasing carrier concentration and temperature [148]. The m^* and v refer to the effective mass and acoustic velocity, respectively. A *saturation* of the thermopower occurs with an increased carrier concentration, e.g. $\sim 10^{18}$ cm^{-3} in p- and n-Si, due to the increased interactions of the electrical carriers with the phonons with a consequent decrease of the mutual drag.

While phonon drag effects were hitherto mainly considered to be a low temperature phenomena [149], recent results in Si NWs were modeled to indicate that they could contribute to a reduced κ [18] and enhanced thermoelectric voltages at much higher temperatures, ~200–300 K. For instance, a κ of ~0.76 W m^{-1} K^{-1} was measured for a 10 nm Si NW (p-type $\sim 10^{19}$ cm^{-3}) [18], much below the bulk value (of 150 W m^{-1} K^{-1}) and even below the theoretically deduced [150] minimum κ of ~1 W m^{-1} K^{-1}. However, these arguments assume that the NW boundary itself is incorporated into the phonon mode. While this study is extremely interesting in that it promises new modes of thought into increasing the thermoelectric figure of merit and efficiency, many details regarding phonon propagation and their contribution to a reduced κ still have to be elucidated.

7.2. Reduced thermal conductivity of Si NWs

Generally, the thermal conductivity, $\kappa \sim Cvl$, where C is the heat capacity per unit volume and v and l are the particle (phonon/electron) velocity and the mean free path [151], respectively. We consider κ to be dominated by the lattice vibrations/phonons as the electronic contribution to the total thermal conductivity is typically much smaller [152]. At the very outset, the κ of Si NWs could either be (a) enhanced from the bulk value of Si due to a reduced phase space for phonon scattering, as was proposed for carbon nanotubes [153], or (b) diminished due to reduction in the l [154, 155]. For the former case, phonon confinement [156] has been posited to increase the κ for the smallest diameter (~1 nm) nanowires [157]. The rationale is that the lowest energy (/longest wavelength) mode is affected the most due to the quantum confinement and dominates thermal transport leading to a concomitant increase in the l and κ. However, most experimental measurements to date have been attempted on Si NWs of diameters >20 nm [18, 158, 159], where κ has been reduced drastically below the bulk value presumably due to a lower l.

For example, at 300 K, the κ of a 115 nm diameter Si NW was measured to be ~40 W m^{-1} K^{-1} and for a 22 nm diameter NW to be ~8 W m^{-1} K^{-1} [158]. It was also noted through the temperature variation of κ that the maxima was shifted to higher temperatures with decreasing NW diameter, e.g. for bulk Si, the peak was at 25 K, while for the 37 nm diameter NW, the κ peak was at 210 K. As the peak indicates the onset of Umklapp scattering, the above results were interpreted as due to the increased influence of the boundary scattering

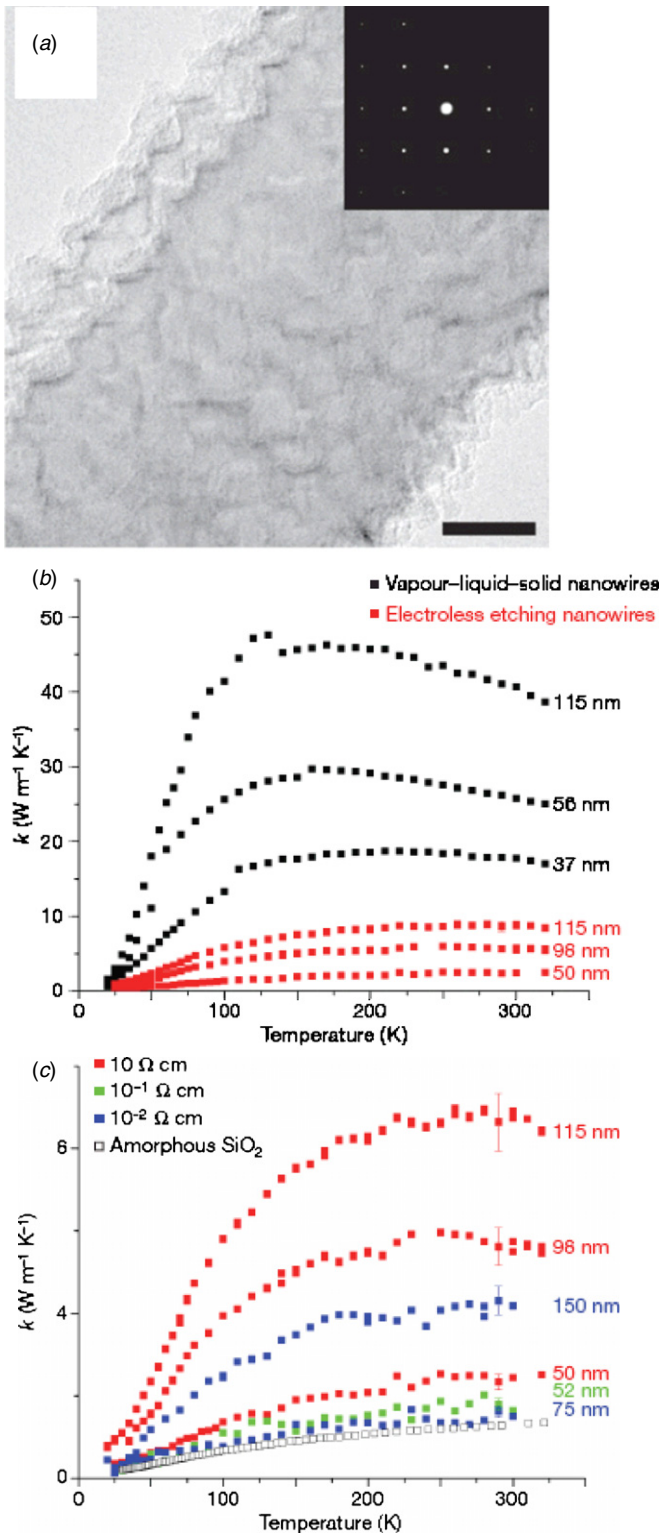

Figure 10. (*a*) Rough Si NWs fabricated through an electroless etching (EE) method. (*b*) The κ decreases with diameter and seems to be a strong function of the NW roughness and the method of synthesis (VLS: vapor–liquid–solid mechanism versus EE: electroless etching). (*c*) An increased dopant–phonon scattering (at lower wafer resistivity) also seems to contribute to a reduced κ. Figures adapted from [159].

for smaller diameter NWs. (Umklapp processes are three-phonon scattering processes which contribute to the bulk κ—

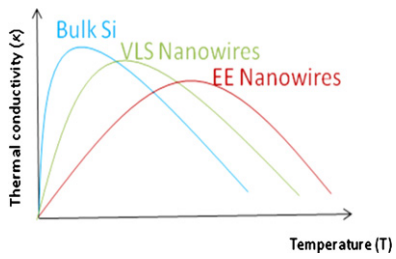

Figure 11. Schematic variation of the thermal conductivity, κ, with temperature (T) as a function of size and increasing roughness (EE > VLS > bulk).

their enhanced temperature onset suggests that alternative processes, e.g. phonon-surface scattering, are important at lower temperatures.) It was also seen that the κ in the range 20 K $< T <$ 100 K varied linearly with the temperature, T [160], for Si NWs of diameters <30 nm. Such a variation for κ could be understood through the dependence of the specific heat, C. For example, in three-dimensional heat conduction C, and hence κ, has been shown to have a T^3 dependence—analogously, for one-dimensional systems C, and κ, would vary linearly with T [161].

Surface roughness of the Si NW at the 1 nm length scale, e.g. induced through oxide formation, has been posited as another variable that could influence phonon transport and κ. Phonon modes whose wavelengths (λ_{ph}) are greater than the NW surface roughness undergo wavelength-/frequency-dependent specular scattering [160] with a mean free path directly proportional to the wavelength. Note that the dominant thermal λ_{ph} $\left(\sim\frac{hv}{k_B T}\right)$ for Si (where the acoustic velocity, $v \sim 9 \times 10^3$ m s^{-1}) at $T = 300$ K is ~1 nm. At lower temperatures, when $\lambda_{ph} \gg$ NW diameter, a ballistic transport regime is reached with a corresponding quantization of the thermal conductance at $\frac{\pi^2 k_B^2 T}{3h}$ ($= 9.456 \times 10^{-13}$ W K^{-2}) T [162].

Consequently, measurements on roughened Si NWs (20–300 nm in diameter, mean roughness ~1–5 nm, figure 10(*a*)) yielded values of κ ~1.2 W m^{-1} K^{-1}, very close to that of amorphous SiO_2 [159] and the theoretically calculated minimum of ~1 W m^{-1} K^{-1} [150]. The NWs were fabricated through an electroless etching (EE) method where a Si wafer was locally oxidized using an aqueous solution of $AgNO_3$ and HF. As expected, the κ decreased with the NW diameter possibly due to a reduced l and enhanced boundary scattering. In addition to the diameter and roughness, the κ was also seen to be dependent on the method of synthesis and resistivity of the initial Si wafer as indicated in figures 10(*b*) and (*c*). A reduction of κ by a factor of 5 was obtained for the EE-synthesized NWs compared to the relatively smooth Si NWs synthesized by the VLS (vapor–liquid–solid) method (section 2.2). The peak of the κ–T curve also shifts with increasing roughness from bulk Si (~5 K) → VLS fabricated nanowires → EE fabricated nanowires—figure 11. Since the peak is indicative [163] of the magnitude of the Debye temperature and onset of Umklapp scattering, it can be surmised that (i) the stiffness of the NWs is increased relative to the bulk and that (ii) the roughness promotes increased surface scattering. Additionally, the κ for Si NWs synthesized with a saw tooth morphology [164] (with cross-sectional areas in the range of 2.58–28.62 nm^2) and core–shell NWs [165] was shown to be two orders of magnitude smaller than bulk Si due to an increased number of diffuse reflections and inelastic scattering [155].

Such studies on Si NWs have brought forward qualitatively the concept of reducing κ through phonon scattering at different length scales, i.e. due to (1) NW diameter, through boundary scattering, (2) surface roughness, for longer wavelength phonon scattering and (3) atomic scattering, e.g. through Si isotope, i.e. Si^{29} or Si^{42}, doping [166]—for short wavelength phonons. The drastic reduction in κ was the primary contributor for the two orders of magnitude increase in the thermoelectric figure of merit (ZT) of Si NWs compared to bulk Si. However, the enhanced ZT of ~1 is still comparable to currently used thermoelectric materials and alternative methods of increasing the efficiency are being studied [167].

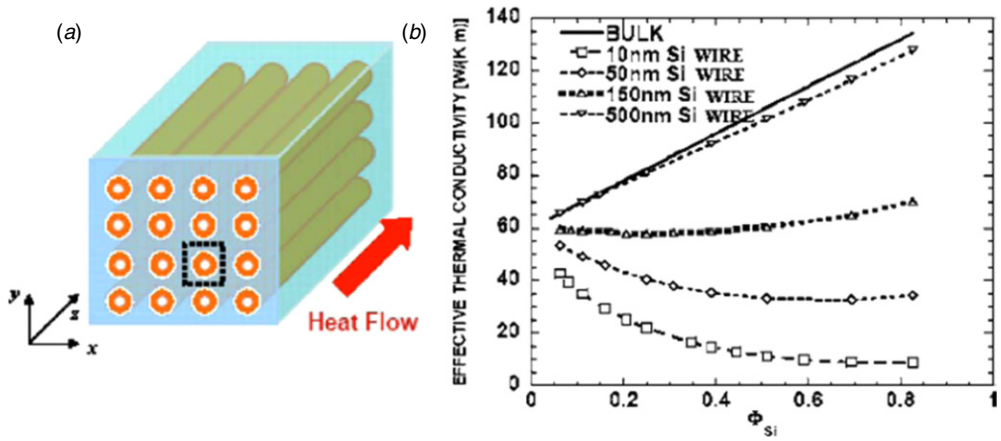

Figure 12. (*a*) Periodic two-dimensional nanocomposites with tubular nanowire inclusions and (*b*) κ reduction to below the bulk value as a function of the silicon nanowire radius (10 nm, 50 nm, 150 nm and 500 nm) and the volumetric ratio (Φ_{Si}) of the silicon nanowires. Figure adapted from [171].

The thermal boundary resistance [168] which characterizes the external NW interactions, say with other NWs, contacts, etc could also be modified through phonon scattering [169]. This implies, for example, that Si NW bundles could have a lower κ compared to a single NW [170]. For two-dimensional nanocomposites (figure 12(*a*)), it was shown that for a given volume fraction of embedded Si NWs (Φ_{Si}) in a Ge bulk matrix, a greater κ reduction could be obtained for smaller diameter NWs [171]. Such a decrease is mainly due to enhanced phonon scattering at the Si–Ge interface, the area of which increases with decreasing NW diameter and the additional influence of surface states (section 3).

8. Conclusions

Si NWs are a manifestation of the influence of nanoscience and technology on one of the most widely studied bulk materials of the past few decades. In this paper, we have outlined salient features of these nanostructures with an emphasis on various methods of synthesis and their characteristic properties. The possibilities of miniaturization have been used to apply Si NWs for electronic devices, photovoltaics, battery electrode materials, thermoelectrics, etc with a goal of improved efficiency in performance and power consumption. Other aspects relevant to the size reduction such as giant piezoresistance in Si NWs [66] and their use as ultra-sensitive nano-electro-mechanical systems (NEMS) [172, 173] could be pertinent for high resolution and mass sensitivity applications. However, the aspect of semiconducting Si NWs that seems to be most interesting from the point of view of developing new scientific and technological paradigms involves quantum confinement. It was seen that such paradigm development mandates Si NWs of sub-5 nm diameters, the controlled and large-scale synthesis of which seems to be quite challenging at the present. Additionally, as with most nanotechnology which requires controlled placement of nanostructures, the growth and arrangement of such small diameter NWs is non-trivial. It is then thought that studies focused on the science of Si NWs are crucial, prior to deciding whether the technological effort on large-scale assembly is necessary.

References

[1] Moore G E 1965 *Electron. Lett.* **38** 4–7
[2] Kumar V 2008 *Nanosilicon* (San Diego, CA: Elsevier)
[3] Iijima S 1991 *Nature* **354** 56–8
[4] Perepichka D F and Rosei F 2006 *Small* **2** 22–5
[5] Collins P G and Avouris P 2000 *Sci. Am.* December 62–9
[6] De Crescenzi M, Castrucci P, Scarselli M, Diociaiuti M, Chaudhari P S, Balsubramanian C, Bhave T M and Bhoraskar S V 2005 *Appl. Phys. Lett.* **86** 231901
[7] Tang Y H, Pei L Z, Chen Y W and Guo C 2005 *Phys. Rev. Lett.* **95** 116102
[8] Dresselhaus M S, Dresselhaus G and Jorio A 2004 *Ann. Rev. Mater. Res.* **34** 247–78
[9] Yang X and Ni J 2005 *Phys. Rev.* B **72** 195426
[10] Guzman-Verri G G and Lew Yan Voon L C 2007 *Phys. Rev.* B **76** 075131
[11] Durgun E, Tongay S and Ciraci S 2005 *Phys. Rev.* B **72** 075420
[12] Hu W, Yoon F, Regonda S, Fernandes P, Vogel E M, Buyukserin F, Zhao X-M and Gao J 2008 Lithographically defined Si nanowire field effect transistors for biochemical sensing *IEEE Int. Conf. on Nanotechnology*
[13] Harriott L R 1999 SCALPEL: projection electron beam lithography *Proc. 1999 Particle Accelerator Conf.* (New York)
[14] Tseng A A, Chen K, Chen C D and Ma K J 2003 *IEEE Trans. Electron. Packag. Manuf.* **26** 141–9
[15] Melosh N A, Boukai A, Diana F, Gerardot B, Badolato A, Petroff P M and Heath J R 2003 *Science* **300** 112–5
[16] Morton K J, Nieberg G, Bai S and Chou S Y 2008 *Nanotechnology* **19** 345301
[17] Heath J R 2008 *Acc. Chem. Res.* **41** 1609–17
[18] Boukai A I, Bunimovich Y, Tahir-Kheli J, Yu J-K, Goddard W A III and Heath J R 2008 *Nature* **451** 168–71
[19] Wang D, Sheriff B A, McAlpine M C and Heath J R 2008 *Nanoresearch* **1** 9–21
[20] Green J E *et al* 2007 *Nature* **445** 414–7
[21] Wagner R S, Ellis W C, Jackson K A and Arnold S M 1964 *J. Appl. Phys.* **35** 2993–3000
[22] Wagner R S and Ellis W C 1964 *Appl. Phys. Lett.* **4** 89–90
[23] Park W I, Zheng G, Jiang X, Tian B and Lieber C M 2008 *Nanoletters* **8** 3004–9
[24] Morales A M and Lieber C M 1998 *Science* **279** 208–11
[25] Westwater J, Gosain D P, Tomiya S, Usui S and Ruda H 197 *J. Vac. Sci. Technol.* B **15** 554–7
[26] Ozaki N, Ohno Y and Takeda S 1998 *Appl. Phys. Lett.* **73** 3700–2
[27] Kikkawa J, Ohno Y and Takeda S 2007 *Appl. Phys. Lett.* **86** 123109/1–3
[28] Zhang Y F, Tang Y H, Wang N, Yu D P, Lee C S, Bello I and Lee S T 1998 *Appl. Phys. Lett.* **72** 1835–7
[29] Porter D A and Easterling K E 1992 *Phase Transformations in Metals and Alloys* (Cheltenham: Nelson Thornes)
[30] Schmidt V, Wittemann J V, Senz S and Goesele U 2009 *Adv. Mater.* **21** 2681–702
[31] Kanungo P D, Zakharov N, Bauer J, Breitenstein O, Werner P and Goesele U 2008 *Appl. Phys. Lett.* **92** 263107
[32] Schwalbach E J and Voorhees P W 2008 *Nanoletters* **8** 3739–45
[33] Schmidt V, Senz S and Gosele U 2005 *Nanoletters* **5** 931–5
[34] Sze S M and Ng K K 2006 *Physics of Semiconductor Devices* (New York: Wiley)
[35] Kamins T I, Williams R S, Chen Y, Chang Y-L and Chang Y A 2000 *Appl. Phys. Lett.* **76** 562–4
[36] Wang Y, Schmidt V, Senz S and Gösele U 2006 *Nat. Nanotechnol.* **1** 186–9
[37] Kalache P, Roca i Caborracas P and Foncuberta i Morral A 2006 *Japan. J. Appl. Phys.* **45** L190–3
[38] Lensch-Falk J L, Hemesath E R, Perea D E and Lauhon L J 2009 *J. Mater. Chem.* **19** 849–57
[39] Jaccodine R J 1963 *J. Electrochem. Soc.* **110** 524–7
[40] Wu Y, Cui Y, Huynh L, Barrelet C J, Bell D C and Lieber C M 2004 *Nanoletters* **4** 433–6
[41] Takeda S, Ueda K, Ozaki N and Ohno Y 2003 *Appl. Phys. Lett.* **82** 979–81
[42] Yang P 2005 *MRS Bull.* **30** 85–91
[43] Lee S T, Wang N and Lee C S 2000 *Mater. Sci. Eng.* B **A286** 16–23
[44] Zhang R-Q, Lisfshitz Y and Lee S T 2003 *Adv. Mater.* **15** 635–40
[45] Wang N, Yao B D, Chan Y F and Zhang X Y 2003 *Nanoletters* **3** 475–7
[46] Tuan H-Y, Lee D C, Hanrath T and Korgel B C 2005 *Nanoletters* **5** 681–4
[47] Wang F, Dong A, Sun J, Tang R, Yu H and Buhro W E 2006 *Inorg. Chem.* **45** 7511–21

[48] Tuan H-Y, Ghezelbash A and Korgel B A 2008 *Chem. Mater.* **20** 2306–13
[49] Holmes J D, Johnston K P, Doty R C and Korgel B A 2000 *Science* **287** 1471–3
[50] Liu H I, Biegelsen D K, Ponce F A, Johnson N M and Pease R F W 1994 *Appl. Phys. Lett.* **64** 1383–5
[51] Liu H I, Biegelsen D K, Johnson N M, Ponce F A and Pease R F W 1993 *J. Vac. Sci. Technol.* B **11** 2532–7
[52] Kao D-B, McVittie J P, Nix W D and Saraswat K C 1988 *IEEE Trans. Electron Devices* **ED-35** 25–37
[53] Okada R and Iijima S 1991 *Appl. Phys. Lett.* **58** 1662–3
[54] Kao D-B, Saraswat K C, McVittie J P and Nix W D 1985 *IEEE Trans. Electron Devices* **ED-32** 2530–1
[55] Juhasz R, Elfstrom N and Linnros J 2005 *Nanoletters* **5** 275–80
[56] Hochbaum A I, Fan R, He R and Yang P 2005 *Nanoletters* **5** 457–60
[57] Shan Y, Kalkan A A, Peng C-Y and Fonash S J 2004 *Nanoletters* **4** 2085–9
[58] Huang Y, Duan X, Wei Q and Lieber C M 2001 *Science* **291** 630–3
[59] Joselevich E and Lieber C M 2002 *NanoLetters* **2** 1137–41
[60] Englander O, Christensen D, Kim J, Lin L and Morris S J S 2005 *Nanoletters* **5** 705–8
[61] Zhao Y and Yakobson B I 2003 *Phys. Rev. Lett.* **91** 035501
[62] Ohring M 1998 *Reliability and Failure of Electronic Materials and Devices* (San Diego, CA: Academic)
[63] Stratakis E, Misra N, Spanakis E, Hwang D J, Grigoropoulos C P, Fotakis C and Tzanetakis P 2008 *Nanoletters* **8** 1949–53
[64] Markussen T, Rurali R, Brandbyge M and Jauho A-P 2006 *Phys. Rev.* B **74** 245313
[65] Markussen T, Jauho A-P and Brandbyge M 2009 *Phys. Rev.* B **79** 035415
[66] He R and Yang P 2006 *Nat. Nanotechnol.* **1** 42–6
[67] Cui Y, Zhong Z, Wang D, Wang W U and Lieber C M 2003 *Nanoletters* **3** 149–52
[68] Ni C, Chattopadhyay J, Billups W E and Bandaru P R 2008 *Appl. Phys. Lett.* **93** 243113
[69] Bandaru P R and Yablonovitch E 2002 *J. Electrochem. Soc.* **149** G599–G602
[70] Yablonovitch E, Allara D L, Chang C C, Gmitter T and Bright T B 1986 *Phys. Rev. Lett.* **57** 249–52
[71] Ponomareva I, Menon M, Richter E and Andriotis A N 2006 *Phys. Rev.* B **74** 125311
[72] Miyazaki S, Schafer J, Ristein J and Ley L 1996 *Appl. Phys. Lett.* **68** 1247–9
[73] Grove A S 1967 *Physics and Technology of Semiconductor Devices* (New York: Wiley)
[74] Hoffmann S, Utke I, Moser B, Michler J, Christiansen S H, Schmidt V, Senz S, Werner P, Gosele U and Ballif C 2006 *Nanoletters* **6** 622–5
[75] Dieter G E 1986 *Mechanical Metallurgy* (New York: McGraw-Hill)
[76] Elfstrom N, Juhasz R, Sychugov I, Engfeldt T, Karlstrom A E and Linnros J 2007 *Nanoletters* **7** 2608–12
[77] Nichols J A, Saito H, Deck C and Bandaru P R 2007 *J. Appl. Phys.* **102** 064306
[78] Martinez J A, Misra N, Wang Y, Stroeve P, Grigoropoulos C P and Noy A 2009 *Nanoletters* **9** 1121–6
[79] Lin M C, Chu C J, Tsai L C, Lin H Y, Wu C S, Wu Y P, Wu Y N, Shieh D B, Su Y W and Chen C D 2007 *Nanoletters* **7** 3656–61
[80] Fan R, Wu Y, Li D, Yue M, Majumdar A and Yang P 2003 *J. Am. Chem. Soc.* **125** 5254–5
[81] Fan R, Karnik R, Yue M, Li D, Majumdar A and Yang P 2005 *Nanoletters* **5** 1633–7
[82] Leao C R, Fazzio A and da Silva A J R 2007 *Nanoletters* **7** 1172–7
[83] Canham L T, Barraclough K G and Robbins D J 1987 *Appl. Phys. Lett.* **51** 1509–11
[84] Van De Walle C G and Northrup J E 1993 *Phys. Rev. Lett.* **70** 1116–9
[85] Gnutzmann U and Clausecker K 1974 *Appl. Phys.* **3** 9–14
[86] Sanders G D and Chang Y-C 1992 *Appl. Phys. Lett.* **60** 2525–7
[87] Delley B and Steigmeier E F 1995 *Appl. Phys. Lett.* **67** 2370–2
[88] Ma D D D, Lee C S, Au F C K, Tong S Y and Lee S T 2003 *Science* **299** 1874–7
[89] Read A J, Needs R J, Nash K J, Canham L T, Calcott P D J and Qteish A 1992 *Phys. Rev. Lett.* **69** 1232–5
[90] Cui Y, Duan X, Hu J and Lieber C M 2000 *J. Phys. Chem.* B **104** 5213–6
[91] Hoffmann S, Bauer J, Ronning C, Stelzner T, Michler J, Ballif C, Sivakov V and Christiansen S H 2009 *Nanoletters* **9** 1341–4
[92] Colli A, Fasoli A, Ronning C, Pisana S, Piscanec S and Ferrari A C 2008 *Nanoletters* **8** 2188–93
[93] Leao C R, Fazzio A and da Silva A J R 2008 *Nanoletters* **8** 1866–71
[94] Muller R S, Kamins T I and Chan M 2003 *Device Electronics for Integrated Circuits* (New York: Wiley)
[95] Schroder D K 2006 *Semiconductor Material and Device Characterization* (New York: Wiley)
[96] Yablonovitch E and Gmitter T 1986 *Appl. Phys. Lett.* **49** 587–9
[97] Perea D, Lensch J L, May S J, Wessels B W and Lauhon L J 2006 *Appl. Phys.* A **85** 271–5
[98] Fukata N, Chen J, Sekiguchi T, Okada N, Murakami K, Tsurui T and Ito S 2006 *Appl. Phys. Lett.* **89** 203109
[99] Dresselhaus M S, Dresselhaus G, Pimenta M A and Eklund P C 1999 *Analytical Applications of Raman Spectroscopy* (Malden, MA: Blackwell Science)
[100] Nichols J A, Saito H, Hoefer M and Bandaru P R 2008 *Electrochem. Solid State Lett.* **11** K35-K9
[101] Lundstrom M 2000 *Fundamentals of Carrier Transport* (Cambridge: Cambridge University Press)
[102] Lundstrom M and Guo J 2006 *Nanoscale Transitors: Device Physics, Modeling, and Simulation* (New York: Springer)
[103] Suk S D *et al* 2008 *IEEE Trans. Nanotechnol.* **7** 181–4
[104] Weber W M *et al* 2006 *Nanoletters* **6** 2660–6
[105] Fernandez-Serra M-V, Adessi C and Blase X 2006 *Nanoletters* **6** 2674–8
[106] Datta S 1995 *Electronic Transport in Mesoscopic Systems* (New York: Cambridge University Press)
[107] Kikuchi A 1999 *Phys. Status Solidi* A **175** 623–9
[108] Schmid H, Bjork M T, Knoch J, Karg S, Riel H and Riess W 2009 *Nanoletters* **9** 173–7
[109] Kobayashi K 2004 *Phys. Rev.* B **69** 115338
[110] Fox M 2001 *Optical Properties of Solids* (New York: Oxford University Press)
[111] Lyons D M, Ryan K M, Morris M A and Holmes J D 2002 *Nanoletters* **2** 811–6
[112] Iyer S S and Xie Y-H 1994 *Porous Silicon* ed Z C Feng and R Tsu (River Edge, NJ: World Scientific)
[113] Kikkawa J, Takeda S, Sato Y and Terauchi M 2007 *Phys. Rev.* B **75** 245317/1–5
[114] Westover T, Jones R, Huang J Y, Wang G, Lai E and Talin A A 2009 *Nanoletters* **9** 257–63
[115] Kayes B M, Lewis N S and Atwater H A 2005 *J. Appl. Phys.* **97** 114302
[116] Nelson J 2003 *The Physics of Solar Cells* (London: Imperial College Press)
[117] Shockley W and Queisser H J 1961 *J. Appl. Phys.* **32** 510–9
[118] Goncher G and Solanki R 2008 Semiconductor nanowire photovoltaics *Proc. SPIE* **7047** 70470 L-1

[119] Goetzberger A, Hebling C and Schock H-W 2003 *Mater. Sci. Eng.* R **40** 1–46
[120] Tsakalakos L *et al* 2007 *J. Nanophoton.* **1** 013552–10
[121] Yablonovitch E and Cody G D 1982 *IEEE Trans. Electron Devices* **29** 300–5
[122] Peng K, Xu Y, Wu Y, Yan Y, Lee S-T and Zhu J 2005 *Small* **1** 1062–7
[123] Street R A, Qi P, Lujan R and Wong W S 2008 *Appl. Phys. Lett.* **93** 163019
[124] Stelzner T, Pietsch M, Andra G, Falk F, Ose E and Christiansen S 2008 *Nanotechnology* **19** 295203
[125] Zervos M 2008 *Semicond. Sci. Technol.* **23** 075016
[126] Kempa T J, Tian B, Kim D R, Hu J, Zheng X and Lieber C M 2008 *Nanoletters* **8** 3456–60
[127] Leonard F and Tersoff J 1999 *Phys. Rev. Lett.* **83** 5174
[128] Tian B, Zheng X, Kempa T J, Fang Y, Yu N, Yu G, Huang J and Lieber C M 2007 *Nature* **449** 885–9
[129] Kelzenberg M D, Turner-Evans D B, Kayes B M, Filler M A, Putnam M C, Lewis N S and Atwater H A 2008 *Nanoletters* **8** 710–4
[130] Rumke T M, Sanchez-Gil J A, Muskens O L, Borgstrom M T, Bakkers E P A M and Gomez Rivas J 2008 *Opt. Express* 5013–21
[131] Muskens O L, Rivas J G, Algra R E, Bakkers E P A M and Lagendjik A 2008 *Nanoletters* **8** 2638–42
[132] Zhu J, Yu Z, Burkhard G F, Hsu C-M, Connor S T, Xu Y, Wang Q, McGehee M, Fan S and Cui Y 2009 *Nanoletters* **9** 279–82
[133] Yang S-H, Cooper M L, Bandaru P R and Mookherjea S 2008 *Opt. Express* **16** 8306–16
[134] Abruna H D, Kiya Y and Henderson J C 2008 *Phys. Today* 43–7
[135] Obrovac M N and Christensen L 2004 *Electrochem. Solid State Lett.* **7** A93–6
[136] Beattie S D, Larcher D, Morcrette M, Simon B and Tarascon J-M 2008 *J. Electrochem. Soc.* **155** A158–63
[137] Yang J, Winter M and Besenhard J O 1996 *Solid State Ion.* **90** 281–7
[138] Graetz J, Ahn C C, Yazami R and Fultz B 2006 *Electrochem. Solid State Lett.* **6** A194-A7
[139] Chan C K, Peng H, Liu G, McIlwrath K, Zhang X F, Huggins R A and Cui Y 2008 *Nat. Nanotechnol.* **3** 31–5
[140] Cui L-F, Ruffo R, Chan C K, Peng H and Cui Y 2009 *Nanoletters* **9** 491–5
[141] Vaurette F, Leturcq R, Nys J P, Deresmes D, Grandidier B and Stievenard D 2008 *Appl. Phys. Lett.* **92** 242109
[142] MacDonald D K C 1962 *Thermoelectricity: An Introduction to the Principles* (Mineola, NY: Dover)
[143] Gurevich L 1945 *J. Phys.* **9** 477–88
[144] Behren E 1990 *J. Appl. Phys.* **87** 287–92
[145] Geballe T H and Hull G W 1955 *Phys. Rev.* **98** 940–7
[146] Herring C 1954 *Phys. Rev.* **96** 1163–87
[147] Behnen E 1990 *J. Appl. Phys.* **87** 287–92
[148] Geballe T H and Hull G W 1954 *Phys. Rev.* **94** 1134–40
[149] Frederikse H P R 1953 *Phys. Rev.* B **92** 248–52
[150] Cahill D G, Watson S K and Pohl R O 1992 *Phys. Rev. B: Condens. Matter* **46** 6131–40
[151] Kittel C 1996 *Introduction to Solid State Physics* (New York: Wiley)
[152] Humphrey T E and Linke H 2005 *Phys. Rev. Lett.* **94** 096601
[153] Kim P, Shi L, Majumdar A and McEuen P L 2001 *Phys. Rev. Lett.* **87** 215502
[154] Lu X 2008 *Appl. Phys. Lett.* **104** 054314
[155] Volz S and Chen G 1999 *Appl. Phys. Lett.* **75** 2056–8
[156] Adu K W, Gutierrez H R, Kuim U J, Sumanasekhara G U and Eklund P C 2005 *Nanoletters* **5** 409–14
[157] Ponomareva I, Srivastava D and Menon M 2007 *Nanoletters* **7** 1155–9
[158] Li D, Wu Y, Kim P, Shi L, Yang P and Majumdar A 2003 *Appl. Phys. Lett.* **83** 2934–6
[159] Hochbaum A I, Chen R, Delgado R D, Liang W, Garnett E C, Najarian M, Majumdar A and Yang P 2008 *Nature* **451** 163–7
[160] Chen R, Hochbaum A I, Murphy P, Moore J M, Yang P and Majumdar A 2008 *Phys. Rev. Lett.* **101** 105501
[161] Prasher R S, Tong T and Majumdar A 2008 *Nanoletters* **8** 99–103
[162] Schwab K, Hendriksen E A, Worlock J M and Roukes M L 2000 *Nature* **404** 974–7
[163] Carruthers P 1961 *Rev. Mod. Phys.* **33** 92–138
[164] Ross F M, Tersoff J and Reuter M C 2005 *Phys. Rev. Lett.* **95** 146104
[165] Prasher R S 2006 *Appl. Phys. Lett.* **89** 063121
[166] Yang N, Zhang G and Li B 2008 *Nanoletters* **8** 276–80
[167] Pichanusakorn P and Bandaru P R 2009 *Appl. Phys. Lett.* **94** 223108
[168] Swartz E T and Pohl R O 1989 *Rev. Mod. Phys.* **61** 605–68
[169] Balandin A A 2005 *J. Nanosci. Nanotechnol.* **5** 1015–22
[170] Maune H, Chiu H-Y and Bockrath M 2006 *Appl. Phys. Lett.* **89** 013109
[171] Yang R, Dresselhaus M S and Chen G 2005 *Phys. Rev.* B **72** 125418
[172] Feng X L, He R, Yang P and Roukes M L 2007 *Nanoletters* **7** 1953–9
[173] He R, Feng X L, Roukes M L and Yang P 2008 *Nanoletters* **8** 1756–61